Design Study and Scaled Experiment of Induction and Synchronous Motor for Civil Application of Electromagnetic Aircraft Launch System

L. Bertola[1], T. Cox, P. Wheeler, S. Garvey, H. Morvan

[1] Institute for Aerospace Technology, The University of Nottingham, Nottingham, NG72TU UK

Abstract— The engine size of modern passenger transport aircraft is principally determined by take-off conditions, since initial acceleration requires maximum engine power. An Electromagnetic Launch (EML) system could provide some or all of the energy required at the launch stage so that the aircraft engine power requirement and fuel consumption may be significantly reduced. So far, EML for aircraft has been adopted only for military applications to replace steam catapults on the deck of aircraft carriers. This paper will describe the application of EML to propel civil aircraft on the runways of modern airports. A comparison of synchronous and asynchronous electrical motor systems designed to launch an A320-200 will be presented. The paper will present the solution of the transient heat transfer problem of EML systems and the respective design limitations of a civil aircraft launcher under rated current density. The experimental setup that will serve for future validation is introduced.

I. Introduction

This paper considers the feasibility of different technologies for an electromagnetic launch (EML) system to assist civil aircraft take-off. This method is investigated to reduce the power required from the engines during initial acceleration which has the potential of reducing noise near airports and improving overall aircraft efficiency through reducing engine thrust requirements. The thrust level that can be delivered by an EML system allows for accelerations that cannot be reached by aircraft engines. Consequently, EML systems have the potential to reduce the nominal runway length required by the aircraft to take-off. Expensive airport extensions to face constant air traffic growth could be avoided by allowing large aircraft to operate from short runways at small airports.

The machine topologies mainly considered for EML are double-sided Linear Induction Motor (LIM) [1] and Linear Permanent Magnet Synchronous Motor (LPMSM) [2]. In order to achieve the high thrust requirement for aircraft launch application and to take advantage of the very short duty cycle required, these machines need to operate with high current density. Most of the electrical machines for continuous operation with similar rated current need significant active cooling of the conductive components. This paper investigates the temperature time evolution inside electromagnetic launchers in order to evaluate the possibility to adopt only passive cooling techniques.

The thermal analysis of the induction motor was carried out in detail for rotary machines [3], while this paper will focus on the transient temperature rise on the active area of the conductive plate of the linear counterpart. The work on LPMSM will look at the eddy current losses into the magnets of the synchronous machine and the consequent limits on armature excitation to avoid demagnetization during operation. Both cases will look at the practical thermal limits on the machine topologies, and how these are best exploited in a highly short term rated application such as civil aircraft launch.

II. Launcher Requirements

General Atomics developed an EML system that is able to launch aircraft up to an F-35C in weight [4]. Table 1 compares the requirements for the military catapult with those for the launch of an A320-200 aircraft.

Table 1: Comparison between military and civil requirements for EML

Requirements	F-35C	A320-200
End speed	78.0 m/s	85.7 m/s
Aircraft mass	37000 kg	73500 kg
Acceleration	3.3 g	0.6 g
Peak Thrust	1198 kN	502.9 kN
Runway length	94 m	624 m
Acceleration time	2.40 s	14.57 s

The end-speed design requirement for the civil aircraft launcher was established considering a factor 1.15 with respect to the speed at which the aircraft detaches. The mover of the catapult disconnects when the aircraft reaches the nose rotation speed. The nose rotation speed was determined considering the aerodynamic performances which allow the aircraft to take-off safely in one engine inoperative conditions. The engine thrust decrease in hot-day conditions was considered as well.

The acceleration of 0.6 g was selected to guarantee an appropriate level of comfort to the passengers considering the maximum axial acceleration safety limits [5].

III. Electromagnetic Design of LIM and LPMSM

The electromagnetic performance of the asynchronous launcher is estimated on the basis of the equivalent circuit model of a LIM whereas the LPMSM was sized with the aid of the d-q phasor model and applying the multi-layer theory as indicated in [6].

Table 2: Comparison between LIM and LPMSM

Parameter	LIM	LPMSM
Peak Efficiency	0.926	0.998
Power Factor	0.586	0.719
End-Thrust [kN]	524	518
Peak Input Power [MW]	82.8	61.8
Armature mass [kg]	869	2498
Pole pitch [m]	0.60	0.154
Stack width [m]	2.0	2.0
Airgap length [mm]	7	7
Aluminum thickness [mm]	20	-
Magnet thickness [mm]	-	40.7
Active pole pairs	3	14
Slot per pole per phase	4	3/7
Current density [A/mm^2]	50	50
Peak Frequency [Hz]	74	278
Thrust density [Pa]	70560	58200

IV. Current Density Limit of the Stator Windings

The rated current density on the primary stator windings in Table 2 is considerably higher than the usual limit of electrical machine without active cooling for continuous operation (~4 A/mm^2). However both the machines are formed by several stages each one separately connected to the power supply. The primary current in each stage is fed for the time Δt required by the mover to cross the stage itself (plus the time taken for the machine to develop its magnetic field). Since the aircraft accelerates the mover will spend the longest period over the first stage (~1.26 s). The temperature increase of the first stage can be computed applying the Onderdonk's law as [7]

$$\Delta T = (234 + T_i)\left[10^{33.5(I_1/A_w)^2 \Delta t} - 1\right] \quad (1)$$

where T_i is the initial temperature, I_1 the primary current and A_w the wire area. The results of eq. (1) for several current densities are reported in Figure 1 where the maximum ΔT allowed by the insulation and the ΔT caused by the optimum current density are highlighted.

V. Thermal Analysis of LIM

The thermal heat transfer problem is solved to estimate the temperature evolution of the mover to prevent the creep of the aluminum plate. Creep is the tendency of a material to deform permanently under high mechanical stresses and heat loads especially when they are applied for a long time. Creep is observed in aluminium, provided that the operating temperature exceeds $0.54 \cdot T_M = 504$ K [8], where $T_M = 933$ K is the absolute melting temperature.

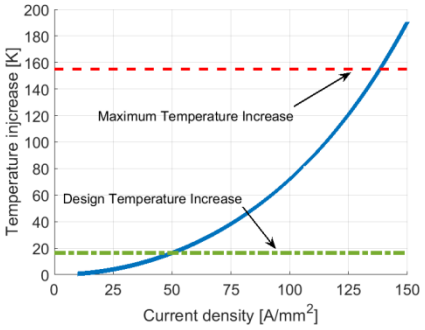

Figure 1 Primary windings temperature increase

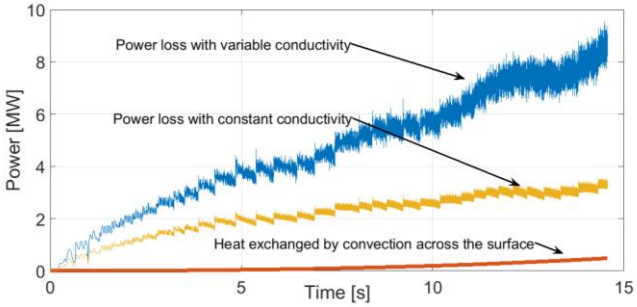

Figure 2: Variation of the secondary Joule losses with time

The temperature of the solid aluminum changes during the launch because of the heat generation due to the induced current and its variation can be described using

$$\rho_{Al} c_{Al} \frac{\partial T}{\partial t} - q_v = \nabla \cdot (k_{Al} \nabla T) \quad (2)$$

where q_v is the volumetric heat generation due to Joule losses and ρ_{Al}, c_{Al} and k_{Al} are the aluminum density, thermal capacity and conductivity respectively. Equation (2) is solved using the implicit finite difference method (FDM) which accounts for the heat exchanged through convection across all the boundaries. The 3D thermal analysis was carried out taking into account the change of the convective coefficient with speed and the electrical conductance of aluminum with temperature.

Heat generations with variable and constant aluminum conductance are compared in Figure 2. The same figures report the heat exchanged through convection across the plate surfaces.

The solution of the heat transfer problem yields the time evolution of the temperature over the aluminum plate volume. The skin effect causes the current density to gather close to the aluminum boundary as the frequency increases during the launch. Therefore, the external layer of the aluminum plate is subject to the most severe thermal conditions. The temperature profile on the lateral surface of the mover at the end of the launch is shown if Figure 3. The creep temperature is never reached being 499.7 K the maximum temperature reached on the plate surface whereas the average temperature of the mover at the end of the launch is 442.9 K.

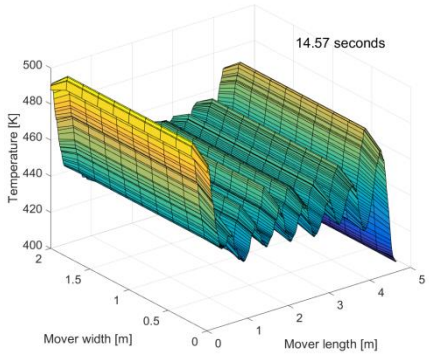

Figure 3: Temperature profile on the mover at the end of the launch

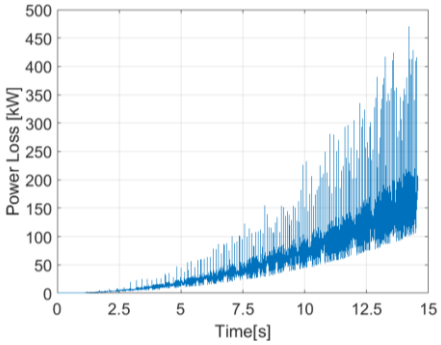

Figure 4: Power loss due to eddy current into the surfaced-mounted PM array

VI. Thermal Analysis of LPMSM

The thermal heat transfer model is applied to LPMSM to determine the temperature change of the surface-mounted magnets during the launch, to prevent demagnetization. Demagnetization may be caused by eddy currents induced by the secondary harmonics of the magnetic wave. The intensity of secondary harmonics is particularly significant in fractional-slot motor like the synchronous launcher under investigation.

Fifty axial and four longitudinal magnet segmentations were implemented to limit the intensity of the induced eddy current. Since the dimensions of a single magnet segment are comparable with the FEA cells the thermal heat transfer problem can be solve analytically applying

$$\rho_{Al} c_{Al} \frac{\partial T}{\partial t} = q_v V_{Mag} \tag{3}$$

where V_{Mag} is the volume of the magnet segment. Conduction is neglected since the magnets are thermally isolated from one to another. Convection is neglected as the convective cooling effect is negligible over the small surfaces exposed to air. The product $q_v V_{Mag}$ represents the total power loss inside a single magnet segment while the total loss due to eddy current in the array of magnets that cover the mover is reported in Figure 4. The spikes in Figure 4 are due to the brisk flux variation that occurs when the mover passes from one stage to another. Solving eq. (3) for a single pole yields a temperature increase of 0.3762 K.

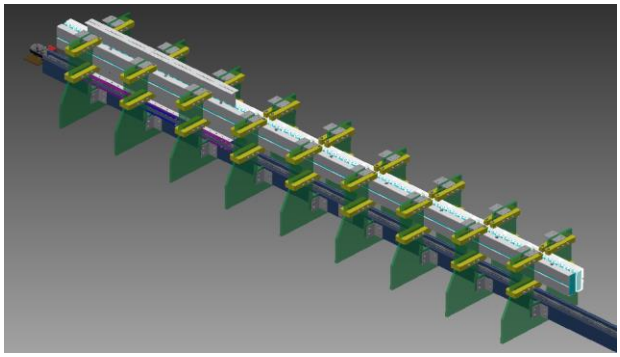

Figure 5: Test rig for experimental validation

VII. Experimental Validation and Conclusion

The optimization of the electromagnetic performance alone does not lead to a viable configuration of EML for civil aircraft application without the thermal validation of the design. The thermal analysis of the LIM limits the dimension of the plate and in particular the plate thickness which is proportional to the plate thermal capacity. The thermal analysis of LPMSM shows that surfaced-mounted magnets do not suffer from thermal demagnetization as long as longitudinal and axial segmentation is applied appropriately.

The analytical results of this paper will be validated with the aid of a thermal camera on the scaled experiment in Figure 5 which was designed employing the same techniques and algorithms used for the civil aircraft launcher.

Acknowledgment

The research leading to these results has received funding from the People Programme (Marie Curie Actions) of the European Union's Seventh Framework Programme (FP7/2007-2013) under REA grant agreement no 608322.

References

[1] G. Bellamy, E. Lewis, "The Development of Advanced Linear Induction Motor Systems," presented at the Power Electronics Machines and Drives, Edinburgh, 2004.

[2] D. Patterson, A. Monti, et al., "Design and Simulation of a Permanent-Magnet Electromagnetic Aircraft Launcher," *IEEE Transaction on Industry Applications*, vol. 41, pp. 566-575, March/April 2005.

[3] Y. Zhang, J. Ruan, T. Huang, X. Yang, H. Zhu, and G. Yang, "Calculation of Temperature Rise in Air-cooled Induction Motors Through 3-D Coupled Electromagnetic Fluid-Dynamical and Thermal Finite-Element Analysis," *IEEE Transactions on Magnetics*, vol. 48, pp. 1047-1050, 2012.

[4] G. Atomics. (2014, October). *EMALS*. Available: http://www.ga.com/emals

[5] ASTM, "Standard Practice for Design of Amusement Rides and Devices," vol. F2291-13, ed, 2014.

[6] L. Bertola, T. Cox, P. Wheeler, S. Garvey, H. Morvan, "Electromagnetic Launch Systems for Civil Aircraft Assisted Take-off," *Archive of Electrical Engineering*, vol. 64, pp. 543-554, 2015.

[7] E. R. Stauffacher, "Short-time current carrying capacity of copper wire," *General Electric Review*, vol. 31, 1928.

[8] S. spigarelli, "Creep of aluminium and aluminium alloys," European Aluminium Association1999.